

# Underplatform Dampers for Turbine Blades: Theoretical Modeling, Analysis, and Comparison With Experimental Data

**K. Y. Sanliturk**

Faculty of Mechanical Engineering,  
Istanbul Technical University,  
80191, Gumussuyu,  
Istanbul, Turkey

**D. J. Ewins**

**A. B. Stanbridge**

Mechanical Engineering Department  
Center of Vibration Engineering,  
Imperial College of Science,  
Technology and Medicine,  
London, SW7 2BX, UK

*This paper describes a theoretical model for analyzing the dynamic characteristics of wedge-shaped underplatform dampers for turbine blades, with the objective that this model can be used to minimize the need for conducting expensive experiments for optimizing such dampers. The theoretical model presented in the paper has several distinct features to achieve this objective including: (i) it makes use of experimentally measured contact characteristics (hysteresis loops) for description of the basic contact behavior of a given material combination with representative surface finish, (ii) the damper motion between the blade platform locations is determined according to the motion of the platforms, (iii) three-dimensional damper motion is included in the model, and (iv) normal load variation across the contact surfaces during vibration is included, thereby accommodating contact opening and closing during vibration. A dedicated nonlinear vibration analysis program has been developed for this study and predictions have been verified against experimental data obtained from two test rigs. Two cantilever beams were used to simulate turbine blades with real underplatform dampers in the first experiment. The second experiment comprised real turbine blades with real underplatform damper. Correlation of the predictions and the experimental results revealed that the analysis can predict (i) the optimum damping condition, (ii) the amount of response reduction, and (iii) the natural frequency shift caused by friction dampers, all with acceptable accuracy. It has also been shown that the most commonly used underplatform dampers in practice are prone to rolling motion, an effect which reduces the damping in certain modes of vibration usually described as the lower nodal diameter bladed-disk modes.*

[DOI: 10.1115/1.1385830]

## 1 Introduction

The friction damping concept is frequently applied in turbomachinery applications, especially at hot locations, to reduce resonance stresses. A typical application of dry friction damping in gas turbines is the so-called "friction damper," "cottage-roof damper," or "underplatform damper," which is loaded by centrifugal force against the underside of the platforms of two adjacent blades. The main design criterion for such devices is to determine the optimum damper configuration or the damper mass or both in order to reduce the dynamic stresses by the maximum possible extent. For example, if the damper mass is too small for a given configuration, the friction force will not be large enough to dissipate sufficient energy. On the other hand, if the damper mass is too large, it will "stick," limiting the relative motion across the interface and thus the amount of energy dissipation. In both cases, the friction damper will be inefficient and between these two extremes there is an optimum size. A good review of the friction damping concept in turbomachinery applications is given by Griffin [1].

The so-called "cottage-roof damper" or "underplatform damper" is physically a very simple device usually a simple-

shaped piece of metal loaded on the underside of adjacent blades. The theoretical analysis and the optimization of these simple devices have been quite difficult, however, due to marked nonlinearity and to uncertainties about the contact characteristics and damper behavior. Substantial effort has been devoted to understanding and modeling basic contact characteristics, usually in the form of friction force-displacement hysteresis loops [2-7].

In addition to those studies related to the basic contact characteristics between two contacting surfaces, several friction damper models and analysis methods have been proposed in the past. The simplest, yet the most commonly used, friction damper model in the literature is the adaptation of a basic macroslip contact model to represent underplatform dampers [8-11]. This simple model is usually combined with a single-degree-of-freedom blade model, the friction damper being attached between the SDOF system and ground. These studies have revealed various important aspects of the friction damper characteristics and yielded some qualitative answers, especially on damping optimization.

More recent research efforts on friction dampers for turbine blades have introduced more details of the damper geometry. Menq et al. [12] have developed a theoretical model for bar-shaped underplatform dampers and that model was used for the forced response analysis of turbine blades [13,14]. Most of the commercially used dampers are more complex than the bar-shaped underplatform dampers. Pfeiffer and Hajek [15] proposed a method to analyze stick-slip vibrations in general and studied a curved wedged damper for turbine blades. The behavior of curved wedge-shaped dampers was also studied by others, usually by approximating the contact behavior using Hertzian contact theory

Contributed by the International Gas Turbine Institute (IGTI) of THE AMERICAN SOCIETY OF MECHANICAL ENGINEERS for publication in the ASME JOURNAL OF ENGINEERING FOR GAS TURBINES AND POWER. Paper presented at the International Gas Turbine and Aeroengine Congress and Exhibition, Indianapolis, IN, June 7-10, 1999; ASME Paper 99-GT-335. Manuscript received by IGTI October 1998; final revision received by the ASME Headquarters, March 1999. Associate Editor: D. Wisler.

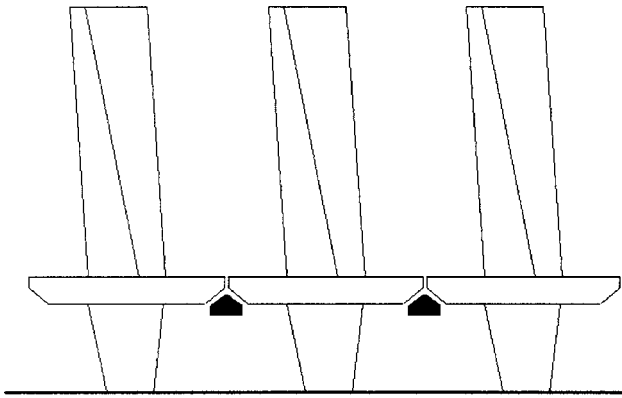


**Fig. 1 Schematic illustration of underplatform dampers between adjacent blades**

[16–18]. The most commonly used type of friction damper in industry is the wedged-shaped damper with flat contact surfaces, as illustrated in Fig. 1 which is also the least studied although important contributions have been made in modeling and analysis of this type of damper [19]. Various analysis methods have also been developed and reported in the literature, mainly for friction damper optimization in turbomachinery applications [11,20–23].

Although significant advances have been made in theoretical modeling of friction dampers and the analysis methods for damper optimization, turbomachine manufacturers still rely on previous experience and empirical data rather than computer-based predictions alone for friction damper optimization. This has been mainly due to the over-simplification introduced in the models regarding the basic contact behavior and/or damper geometry and the inability to analyze representative-size models due to excessive computational cost.

This paper proposes a methodology which combines three essential aspects of friction damping optimization in turbomachinery application. These include (i) utilizing experimentally measured hysteresis loops to describe the basic contact behavior between contacting surfaces in the analysis, (ii) development of a theoretical model for the motion of the wedge-shaped friction dampers and the forces generated at the contact interfaces, and (iii) development of an efficient analysis method which enables the analyst to use realistic finite elements models to describe the dynamic behavior of real turbine blades. The analysis methodology in (iii) is based on a combination of the harmonic balance method and a structural modification approach. The main motivation behind this work is to develop a friction damper optimization technique which is capable of dealing with real geometries.

As our paper addresses almost the same problem studied in [19], it is appropriate here to describe some of the similarities as well as the differences. The work reported here is similar to [19] in the sense that both aim to develop a prediction capability for the optimization of wedge-shaped dampers, the kinematics of the wedge-shaped damper are based on the motion of the platform nodes and the harmonic balance method is applied for the nonlinear analysis. The main differences are that our approach here includes three-dimensional platform and two-dimensional contact motions, microslip type of interface definition, a very efficient numerical analysis procedure and also includes experimental test case using real turbine blades.

## 2 Contact Model

In contrast to most research work in the literature, the contact model used in this work is based on an empirical model whose properties are obtained from experimental data. The experimental test rig reported in [7] for the measurement of hysteresis data has been slightly modified to measure the contact behavior of under-

platform dampers. This was achieved by rubbing a real underplatform damper against a block which was made of the same material as that of the blade with similar surface finishes. These measurements were carried out at constant normal load in order to provide the basic contact properties, although the analysis includes normal load variation during the blade response analysis as will be addressed in Section 3.2. It is noted that the overall contact behavior is quite similar to the “point” contact measurements reported in [7]. Furthermore, it has been found that the hybrid model proposed in [7] is generally adequate to represent the measured hysteresis loops, a typical example of which is illustrated in Fig. 2(a). Also, an array of macroslip elements, as shown in Fig. 2(b) can successfully be used to reproduce the observed microslip behavior [24].

## 3 Friction Damper Model

Underplatform dampers are physically very simple devices, yet their nonlinear behavior is quite complicated and its analysis can be extremely difficult if all the details of the damper characteristics are to be included in the analysis. These difficulties arise due to many complicated factors: for example, the temperature, frequency, and surface roughness effects, the real contact locations and their variation during vibration are just some of them. In spite of the physical simplicity of these dampers, the effects of these and other factors have not yet been fully understood. Accordingly, based on engineering judgement, some simplifying assumptions as listed below have been made here in order to reduce the problem to a manageable level:

- damper flexibility and inertia effects are negligible,
- damper contact on each side can be represented as a point contact with three translational degrees-of-freedom,
- left and right surfaces are identical, and
- the blade motion is harmonic.

In addition to the assumptions above, the first stage of the formulation below will have an additional assumption that

- damper and platform surfaces remain in parallel and in contact at all times.

Experimental results, however, indicated that this last assumption is often not valid for the wedge-shaped dampers studied here, and so some corrections are introduced later.

The friction damper model presented below is based on a given amplitude of vibration and so the model parameters must be recalculated until convergence is achieved due to marked nonlinearity of these devices. The analysis method based on iterative approach is given in Section 4.

**3.1 Relative Motion Across Damper Surfaces.** The theoretical formulation of the cottage roof damper motion as presented here is based on a model as shown in Fig. 3 where a local coordinate system is attached to one of the platforms and the instantaneous relative motion of the other platform is described by

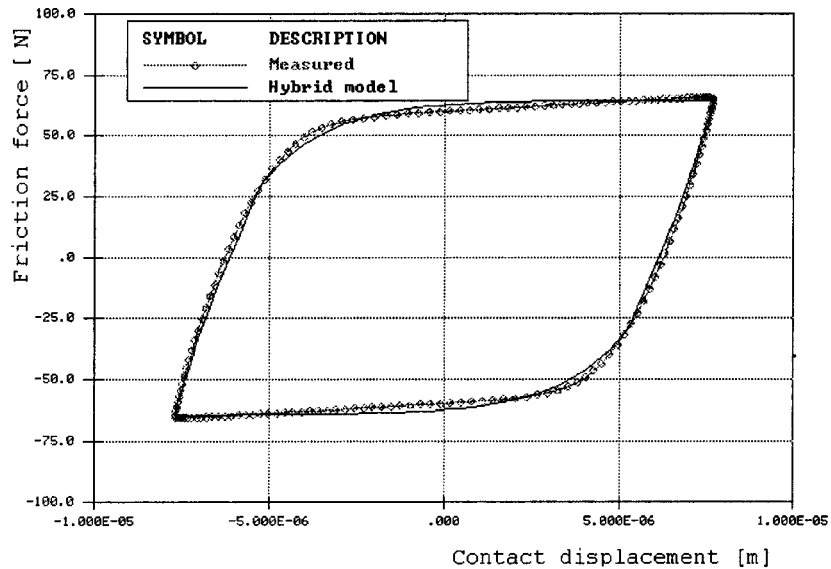
$$\mathbf{r}_{xyz} = \mathbf{i}r_x + \mathbf{j}r_y + \mathbf{k}r_z \quad (1)$$

where

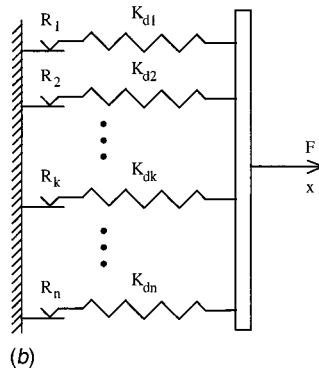
$$\begin{aligned} r_x &= |X| \cos(\omega t + \phi_x) \\ r_y &= |Y| \cos(\omega t + \phi_y) \\ r_z &= |Z| \cos(\omega t + \phi_z) \end{aligned} \quad (2a)$$

and

$$\begin{aligned} X &= X_L - X_R \\ Y &= Y_L - Y_R \\ Z &= Z_L - Z_R. \end{aligned} \quad (2b)$$



(a)



(b)

**Fig. 2 (a) Typical measured hysteresis loop under constant normal load, (b) representation of measured behavior by an array of macroslip elements**

$X_L, Y_L, Z_L, X_R, Y_R, Z_R$  above are complex quantities representing both amplitude and phases at platform nodes. Similarly,  $X, Y,$  and  $Z$  are the relative platform displacements with respect to the local coordinate system,  $\phi_x, \phi_y,$  and  $\phi_z$  being the corresponding phase angles. Furthermore,  $\omega$  is the angular velocity and  $t$  is time. It should be stated at the outset that  $r_x, r_y, r_z$  and other parameters which are functions of them are not constant values but functions of the angular displacement,  $\omega t$ . The damper formulation presented in this paper requires calculation of these dis-

placements (and the associated forces in the next section) for at least one vibration cycle. However,  $\omega t$  is dropped in the equations for brevity.

The relative platform motion in Fig. 4 is three-dimensional, having components in all three local directions. The relative displacements of the underplatform damper with respect to the platform surfaces shown in Fig. 5 are calculated based on the assumption that the centrifugal force acting on the damper mass is large enough to keep the damper in contact with the platform surfaces at all times.

Accordingly, a displacement triangle in Fig. 6 can be drawn

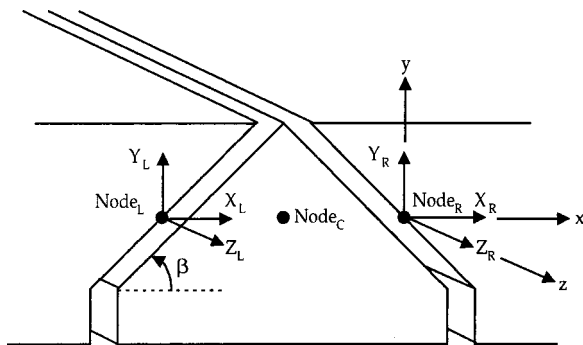


**Fig. 3 Platform motion in three-dimensional space. ( $\beta$  is the platform angle,  $Node_L$  and  $Node_R$  are the platform structural nodes.)**

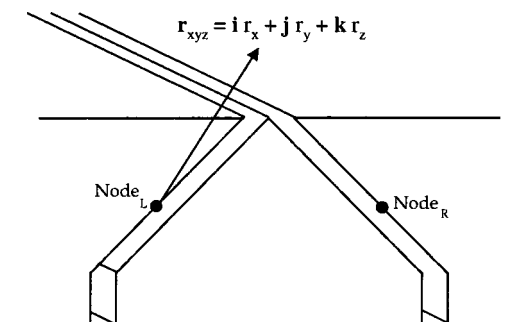


**Fig. 4 Relative platform displacements**

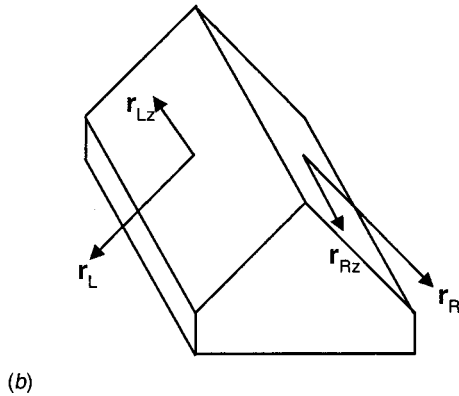
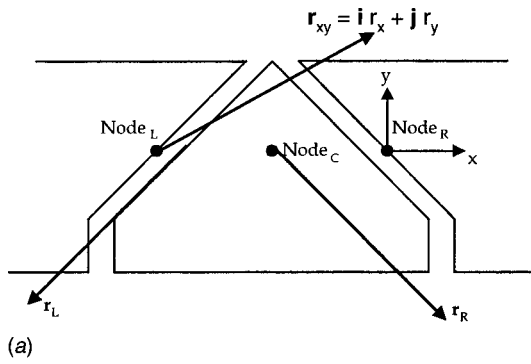


Fig. 5 Relative contact displacements on damper surfaces

relating the relative displacements of the platform in  $x$ - $y$  plane ( $\mathbf{r}_{xy}$ ) and the relative contact displacements  $\mathbf{r}_L$  and  $\mathbf{r}_R$  in Fig. 5(a). Since the directions of all the vectors in Fig. 5(a) and the magnitude of the  $\mathbf{r}_{xy}$  are known, the magnitudes of the  $\mathbf{r}_L$  and  $\mathbf{r}_R$  are calculated as

$$|\mathbf{r}_L| = \frac{|\mathbf{r}_{xy}|(\sin(\alpha) + \cos(\alpha)\tan(\beta))}{2\sin(\beta)} \quad (3a)$$

$$|\mathbf{r}_R| = \frac{|\mathbf{r}_{xy}|\cos(\alpha)}{\cos(\beta)} - |\mathbf{r}_L|. \quad (3b)$$

Another component of the relative contact motion is in the local  $z$ -direction as indicated by  $\mathbf{r}_{Lz}$  and  $\mathbf{r}_{Rz}$  in Fig. 5(b) and there is some uncertainty regarding how the  $\mathbf{r}_z$  is shared between the left and the right-hand side of the damper. It is assumed in this paper that the relative platform motion in the  $z$ -direction is shared equally between left and right side of the damper, i.e.,

$$|\mathbf{r}_{Lz}| = |\mathbf{r}_{Rz}| = |\mathbf{r}_z|/2. \quad (3c)$$

The reasoning behind above assumption is that minimum energy will be dissipated if the two sides share the relative displacements

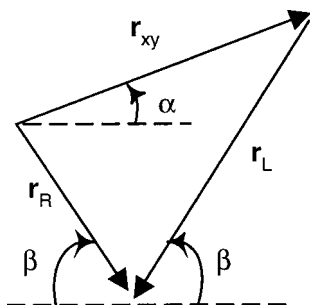


Fig. 6 Displacement triangle relating  $r_{xy}$  to  $r_L$  and  $r_R$

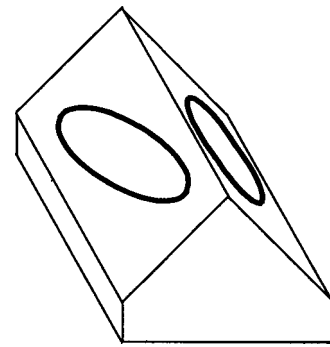


Fig. 7 Damper displacements with respect to the platform surfaces

equally. In general, there is a phase difference between the relative contact displacements in the  $x$ - $y$  plane and in the  $z$ -direction and this results in elliptical relative contact motion as illustrated in Fig. 7. The reader may refer to [24] for details of how to analyze those interfaces where the relative contact motion is elliptical as well as how to relate a one-dimensional microslip model to elliptical motion at the interface.

**3.2 Damper Forces.** Determination of the friction forces across the damper surfaces requires contact displacement and normal load as well as the contact characteristics. The relative contact displacement can be calculated using the procedure summarized above.

The forces on a typical underplatform damper are quite complex in spite of the simplifying assumptions and in spite of the simplicity of the “static” forces involved in Fig. 8 where  $CF$  represents centrifugal force acting on the damper and  $N_{Ls}$  and  $N_{Rs}$  are the static reaction forces in the absence of any vibration. These reaction forces can easily be calculated using the static equilibrium conditions as depicted in Fig. 8(a) and given by

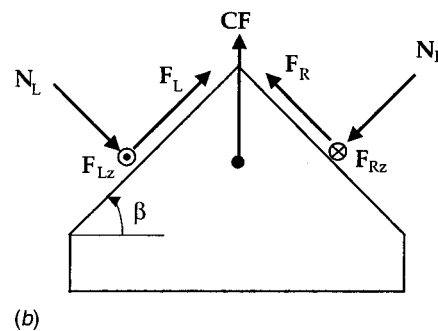
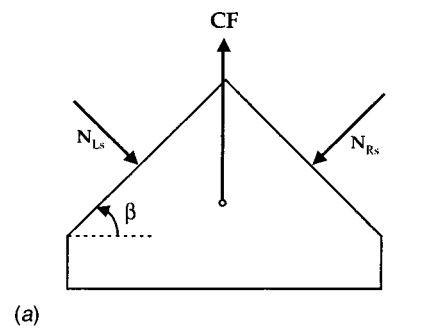


Fig. 8 Forces acting on a damper; (a) static case, (b) dynamic case

$$N_{Ls} = N_{Rs} = N_s = \frac{CF}{2 \cos(\beta)}. \quad (4)$$

The results, not presented here, indicate that the normal forces during vibration can deviate significantly from those of the mean “static” values. The main difficulty in including normal load variations is that the normal loads on the damper surfaces depend on friction forces and vice versa. In Fig. 8(b),  $N_L$  and  $N_R$  are different from each other, as are the corresponding friction forces on each side of the damper. As the damper inertia is neglected, the total force acting on a cottage roof damper must be zero for equilibrium, hence one can write equilibrium equations in local  $x$ - and  $y$ -directions, respectively, at any arbitrary time during a vibration cycle as follows:

$$N_L \sin(\beta) + F_L \cos(\beta) = N_R \sin(\beta) + F_R \cos(\beta) \quad x\text{-dir} \quad (5a)$$

$$N_L \cos(\beta) + N_R \cos(\beta) = F_L \sin(\beta) + F_R \sin(\beta) + CF \quad y\text{-dir}. \quad (5b)$$

It is worth mentioning here that similar to the relative displacements, the dynamically varying forces are functions of the angular displacement,  $\omega t$ , although  $\omega t$  is dropped from these equations. Using Eq. (5), one can write the normal loads on each side of the damper as a function of  $CF$  and the friction forces  $F_L$  and  $F_R$ , as given below.

$$N_L = \frac{(F_L + F_R)}{2} \tan(\beta) + \frac{CF}{2 \cos(\beta)} - \frac{(F_L - F_R)}{2 \tan(\beta)} \quad (6a)$$

$$N_R = \frac{(F_L + F_R)}{2} \tan(\beta) + \frac{CF}{2 \cos(\beta)} + \frac{(F_L - F_R)}{2 \tan(\beta)}. \quad (6b)$$

The dynamic equilibrium condition above provides only two equations and there are four unknowns to be determined, namely:  $N_L$ ,  $N_R$ ,  $F_L$ , and  $F_R$ . (The friction forces in local  $z$ -direction,  $F_{Lz}$  and  $F_{Rz}$  are perpendicular to the normal loads hence they are excluded in determining the normal loads here). Although the normal loads on the contact surfaces and the corresponding friction forces are not independent, it is very difficult to write an explicit relationship between them since this relationship is nonlinear and depends on the previous history of the contact motion. There are two possible solutions to overcome this problem: (i) iterate until convergence is achieved at every increment of a vibration cycle and, (ii) update the normal load successively at every increment of a vibration cycle without iteration. Both of these strategies, (i) and (ii) above, can be used to calculate the normal forces as well as the friction forces. It has been found, however, that option (i) is fairly expensive compared to option (ii) as option (ii) can yield acceptable accuracy. Therefore, only the second approach, also called the successive approximation approach, is described here.

In the so-called successive approximation approach, the normal loads are updated according to the friction forces calculated in a previous step, without involving any iteration. Various steps involved in this approach are summarized below.

Step 1 Start with static normal load (set the angular displacement to zero:  $\theta = \omega t = 0$ )

$$N_L = N_R = \frac{CF}{2 \cos(\beta)}. \quad (4')$$

Step 2 Calculate  $F_L$ ,  $F_R$ ,  $F_{Lz}$ ,  $F_{Rz}$  based on  $N_L, N_R$ .

Step 3 Calculate new normal loads using equilibrium equation

$$N_L = \frac{(F_L + F_R)}{2} \tan(\beta) + \frac{CF}{2 \cos(\beta)} - \frac{(F_L - F_R)}{2 \tan(\beta)} \quad (6a)$$

$$N_R = \frac{(F_L + F_R)}{2} \tan(\beta) + \frac{CF}{2 \cos(\beta)} + \frac{(F_L - F_R)}{2 \tan(\beta)}. \quad (6b)$$

Step 4 If  $\theta = 4\pi$ , exit the cycle, otherwise set  $\theta = \theta + \Delta\theta$  and go to Step 2.

It is obvious that there is some approximation involved in this approach. The normal loads used to calculate the current friction forces are in fact “correct” values for the previous step. That is to say that “correct” normal loads lag the friction forces by one angular increment and the error introduced due to this is found to be less than 5 percent when  $\Delta\theta = \pi/36$ . The 5 percent quoted here is the maximum error value obtained after comparing the correct and the approximate results for many combinations and levels of platform motion and contact parameters.

Whether the iterative or the successive approximation approach is employed, it is necessary to be able to calculate the friction forces while normal loads vary during a vibration cycle, i.e., Step 2 above. This is carried out as follows. The hybrid type of point contact model proposed in [7] is represented by an array of macroslip element as shown in Fig. 2(b) [24]. The initial properties of the model—namely, the individual stiffness values ( $K_{dk}$ ) and the corresponding limiting friction forces ( $R_k$ )—are calculated based on measured contact stiffness and the coefficient of friction and the static normal load  $N_s$  for a given maximum amplitude of vibration. These sliders are then traced, as described in Ref. [24], across the damper surfaces while the individual limiting friction forces are adjusted as the normal loads on each side of the damper vary during a vibration cycle. For example, for the left side

$$R_k = R_{ks} \frac{N_L}{N_s} \quad k = 1, 2, \dots, n \quad (7)$$

where  $R_{k,r}$  is the limiting friction force for the  $k$ th element based on static normal load and  $n$  is the number of sliders used in the model. This tracing process is carried out for a few cycles (usually two) until the trajectories of the sliders are stabilised and this allows the calculation of the friction forces ( $F_L, F_{Lz}, F_R, F_{Rz}$ ) as well as the normal loads ( $N_L, N_R$ ) acting on the damper.

## 4 Analysis Method

The analysis method proposed in this paper is a combination of the harmonic balance method and a structural modification approach and the proposed approach here is designed particularly for analyzing large models with localized nonlinearities very efficiently.

The behavior of the friction damper is analyzed at a given relative response amplitude between the damper connection points and the individual dampers are linearised as equivalent complex stiffnesses, representing both restoring and energy dissipation characters. This is addressed in Section 4.1 below for the underplatform damper described in Section 3. Section 4.2 describes the second stage where these equivalent complex stiffnesses are added to the otherwise linear system to include the effect of the friction dampers. The iterative nature of the problem as well as the procedure to analyze nonlinear systems at active coordinates only, are also described. It must be noted, however, that the nonlinear analysis procedure presented here is not limited to the friction dampers only. The methodology can easily be applied for the analysis of structures with other types of nonlinearities.

**4.1 HBM Linearization of Damper Forces.** After the normal and the corresponding friction forces are determined, the resulting forces applied to Node<sub>L</sub> in Fig. 9 can be decomposed into  $x$ -,  $y$ - and  $z$ -directions as:

$$F_{Lx}(\theta) = F_L(\theta) \cos(\beta) + N_L(\theta) \sin(\beta) \quad (8a)$$

$$F_{Ly}(\theta) = F_L(\theta) \sin(\beta) - N_L(\theta) \cos(\beta) \quad (8b)$$

$$F_{Lz}(\theta) = F_{Lz}(\theta) \quad (8c)$$

A similar set of equations can also be written for at Node<sub>R</sub>. Note that  $F_L, N_L$  (and others) in the above equations are expressed as  $F_L(\theta)$  and  $N_L(\theta)$  in order to emphasise that they are not constant but are functions of  $\theta$  and they are defined for a vibration cycle.

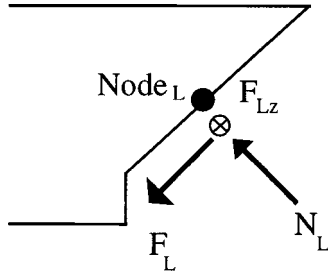


Fig. 9 Dynamic forces acting on the left platform

The first-order components of the resulting forces in the  $x$ -,  $y$ - and  $z$ -directions are calculated and scaled to obtain a complex stiffness representation of these forces in a manner similar to that for the one-dimensional case, as in [23]. For example, the effect of the friction damper in the  $x$ -direction is represented by a complex stiffness ( $k_x^* = k_x^r + ik_x^i$ ) between the platform nodes as

$$k_x^r = \frac{1}{\pi|X|} \int_0^{2\pi} F_{Lx}(\theta) \cos(\theta + \phi_x) d\theta$$

$$k_x^i = \frac{-1}{\pi|X|} \int_0^{2\pi} F_{Lx}(\theta) \sin(\theta + \phi_x) d\theta. \quad (9a)$$

Similarly, the equivalent stiffness in  $y$  and  $z$ -directions are

$$k_y^r = \frac{1}{\pi|Y|} \int_0^{2\pi} F_{Ly}(\theta) \cos(\theta + \phi_y) d\theta,$$

$$k_y^i = \frac{-1}{\pi|Y|} \int_0^{2\pi} F_{Ly}(\theta) \sin(\theta + \phi_y) d\theta \quad (9b)$$

$$k_z^r = \frac{1}{\pi|Z|} \int_0^{2\pi} F_{Lz}(\theta) \cos(\theta + \phi_z) d\theta,$$

$$k_z^i = \frac{-1}{\pi|Z|} \int_0^{2\pi} F_{Lz}(\theta) \sin(\theta + \phi_z) d\theta. \quad (9c)$$

As  $F_{Lx}(\theta)$ ,  $F_{Ly}(\theta)$ , and  $F_{Lz}(\theta)$  are known at discrete values of  $\theta$ , numerical integration can be carried out easily for the integrals in above equations.

**4.2 Analysis Method.** The solution procedure adopted in the frequency domain is based on finding the response amplitudes iteratively, the starting point being the response levels of the underlying linear system. The behavior of the friction dampers is analyzed at a given relative response amplitude between the damper connection points and the individual dampers are represented as equivalent complex stiffnesses, representing both restoring and energy dissipation characteristics as described above. The equivalent complex stiffnesses are then added to the otherwise linear system and the response levels of the modified system are calculated again, the procedure being repeated until convergence is achieved. The response levels obtained at current frequency are used as initial guesses for the next frequency increment.

A very efficient analysis method is proposed here for the analysis of systems with localized nonlinearities via a structural modification approach. An important feature of the method here is that it treats the linear and the nonlinear parts of a structure separately, the linear part being the original structure and the nonlinear part representing the modifications. The nonlinear elements (modifications) are linearised as equivalent stiffnesses at given amplitude of vibration using the first-order HBM as in the previous section. Expressing the nonlinearities as an impedance matrix multiplied by the displacement amplitude vector, was proposed earlier in [25–27] where the method developed by Ozguven [28] for the

harmonic response analysis of nonproportionally damped linear structures was adopted for harmonic response analysis of nonlinear structures. The mathematical background of the approach in this current paper is different; it is based on the Sherman-Morrison formula [29] and it is more general and more efficient for studying nonlinear systems than the method in [28]. The Sherman-Morrison formula has been used in the past [30] to calculate the frequency response of a (linear) modified structure. However, to the best of the authors' knowledge, this paper is the first to propose this method for the analysis of nonlinear systems and it has very good potential for the analysis of wide range of structures. It is shown in [29] that the Sherman-Morrison formula allows a direct inversion of the modified matrix efficiently using the data related to the initial matrix and to the modification. A brief summary of the Sherman-Morrison formula is given below.

Let  $[A]^{-1}$  be the inverse of a nonsingular square matrix,  $[A]$ . If the inverse of a modified matrix,  $[A']^{-1}$ , is needed where  $[A']$  is of the form

$$[A'] = [A] + \{u\}\{v\}^T. \quad (10)$$

This can be calculated using the Sherman-Morrison formula without any matrix inversion as

$$[A']^{-1} = [A]^{-1} - \frac{([A]^{-1}\{u\})(\{v\}^T[A]^{-1})}{1 + \lambda} \quad (11)$$

where

$$\lambda = \{v\}^T [A]^{-1} \{u\}. \quad (12)$$

The generalization of Eq. (11) is also available and is known as Sherman-Morrison-Woodbury formula which considers the modification as a product of two rectangular matrices such as  $[U] \times [V]^T$ . A more detailed coverage including the history of these formulas and the numerical aspects are discussed in [29].

It is proposed in this paper to adopt the Sherman-Morrison formula to calculate the nonlinear response levels of structures with localized nonlinearities rather than the linear modification analysis as reported in [30]. This is achieved as follows. Suppose that the linear structure is given by its dynamic stiffness matrix  $[Z]$  and its frequency response function matrix  $[\alpha]$ ,  $[\alpha] = [Z]^{-1}$ , and the modification matrix to be made to  $[Z]$  is  $[\Delta]$ . The dynamic stiffness matrix of the modified system  $[Z']$ , can then be written as

$$[Z'] = [Z] + [\Delta]. \quad (13)$$

If the modification matrix is written in the form

$$[\Delta] = \{u\}\{v\}^T, \quad (14)$$

the FRF matrix of the modified system  $[\beta]$  can be computed from

$$[\beta] = [Z']^{-1} = [\alpha] - \frac{([\alpha]\{u\})(\{v\}^T[\alpha])}{1 + \{v\}^T[\alpha]\{u\}} \quad (15)$$

which allows the FRF matrix of the modified system to be calculated without any matrix inversion. It should be noted that if the total modification matrix  $[\Delta]$  cannot be written as a multiplication of two vectors as in Eq. (13), it can be decomposed into several, say  $p$ , modification matrices, such as

$$[\Delta] = [\Delta_1] + [\Delta_2] + [\Delta_3] + \dots + [\Delta_p] \quad (16)$$

where  $[\Delta_i] = \{u_i\}\{v_i\}^T$ . This allows the FRF of the system to be calculated by considering each  $[\Delta_i]$  individually. For example, the spring modification in local  $x$ ,  $y$  and  $z$ -directions in Eq. (9) can be included one at a time. It should be stated, however, that it is necessary to transform the individual stiffnesses from the local to a global coordinate system (GCS) as these coordinate systems, in general, do not coincide. This transformation also results in individual modification matrices being in the form of  $\{u_i\}\{v_i\}^T$  as illustrated below in the case of  $x$ -direction:

$$\begin{aligned}
[k]_{6 \times 6} &= k_x^* \begin{bmatrix} e^2 & fe & ge & -e^2 & -fe & -ge \\ ef & f^2 & gf & -ef & -f^2 & -gf \\ eg & fg & g^2 & -eg & -fg & -g^2 \\ -e^2 & -fe & -ge & e^2 & fe & ge \\ -ef & -f^2 & -gf & ef & f^2 & gf \\ -eg & -fg & -g^2 & eg & fg & g^2 \end{bmatrix} \\
&= \begin{pmatrix} e \\ f \\ g \\ -e \\ -f \\ -g \end{pmatrix} \begin{pmatrix} e \cdot k_x^* \\ f \cdot k_x^* \\ g \cdot k_x^* \\ -e \cdot k_x^* \\ -f \cdot k_x^* \\ -g \cdot k_x^* \end{pmatrix} = \{u_i\} \{v_i\}^T \quad (17)
\end{aligned}$$

where  $k_x^*$  is the equivalent complex stiffness in the local  $x$ -direction,  $[k]_{6 \times 6}$  is the modification matrix corresponding to the translations at platform nodes with respect to the GCS, and  $e, f, g$  are the direction cosines of the local  $x$ -direction.

Another distinct feature of the technique proposed here is that the analysis can be restricted to active coordinates only; the active coordinates being the nonlinear coordinates, forcing coordinates and those coordinates where response levels are needed. This is achieved by using the natural frequencies and mode shapes of the linear system in order to describe the frequency response functions at active coordinates via modal summation. This feature has made it possible to analyse industrial cases, as the analysis does not depend on the size of the original linear model.

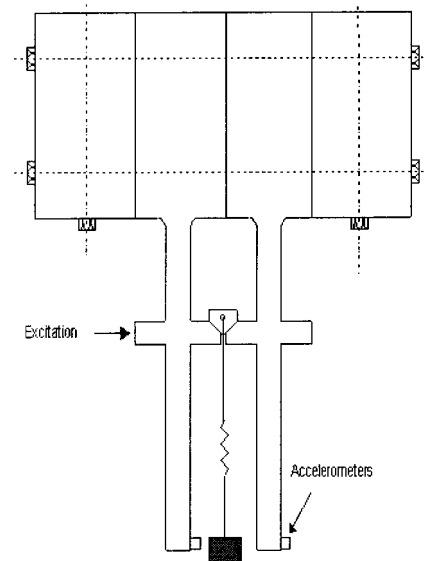
## 5 Predictions and Comparison With Experimental Data

### 5.1 Case 1: Simplified Blade-Damper-Blade Assembly

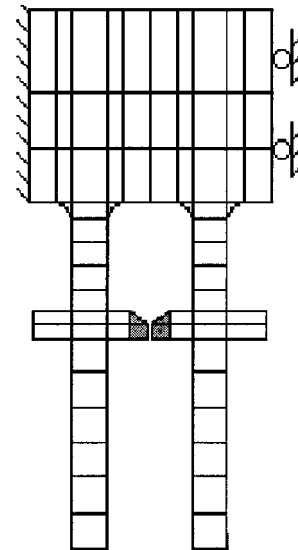
The test rig, schematically illustrated in Fig. 10(a) essentially comprised two beams representing blades with representative platforms so as to accommodate an industrial wedge-shaped underplatform damper. The cantilever beams were clamped together via two clamping blocks and the whole assembly was in turn clamped to a large seismic block, the clamping arrangement being identical to that described in Ref. [31]. An industrial underplatform damper was installed between the blades about 33 percent up from the built-in ends and mass loading was applied so as to represent centrifugal load. Stepped-sine frequency response testing was carried out using constant input force levels. Nonlinear response levels were measured for various damper loads within a frequency range which covered the first two bending modes of the assembly, i.e., the in-phase (IP) and out-of-phase (OOP) bending modes of the two-beam assembly.

The linear structure was modelled using two-dimensional isoparametric plane elements, including the curvature at the root, as shown in Fig. 10(b). The clamping blocks were not included in the finite element model. Instead, fixed-displacement boundary conditions, shown in Fig. 10, were imposed so as to represent the linear behavior of the system. Correlation of the predictions and the measurements for the linear system was found to be quite good as illustrated in Fig. 11. It is important to note in Fig. 11 that there are two close bending modes around 530 Hz, i.e., in-phase (IP) and out-of-phase (OOP) bending modes, respectively.

The first set of results was calculated for a range of damper loads as in the experiments, the excitation force being maintained at 1.0 N amplitude. For comparison purposes, the predicted nonlinear response amplitudes, at the tips of the blades, were overlaid with measured values, as shown in Fig. 12 which contains a series of initially predicted and measured responses at different damper loads, but for the same level of excitation. Inspection of the results in Fig. 12 reveals that the theoretical predictions are rather different to the measured response levels. The most important point to note is that the measured natural frequency shift for the first mode



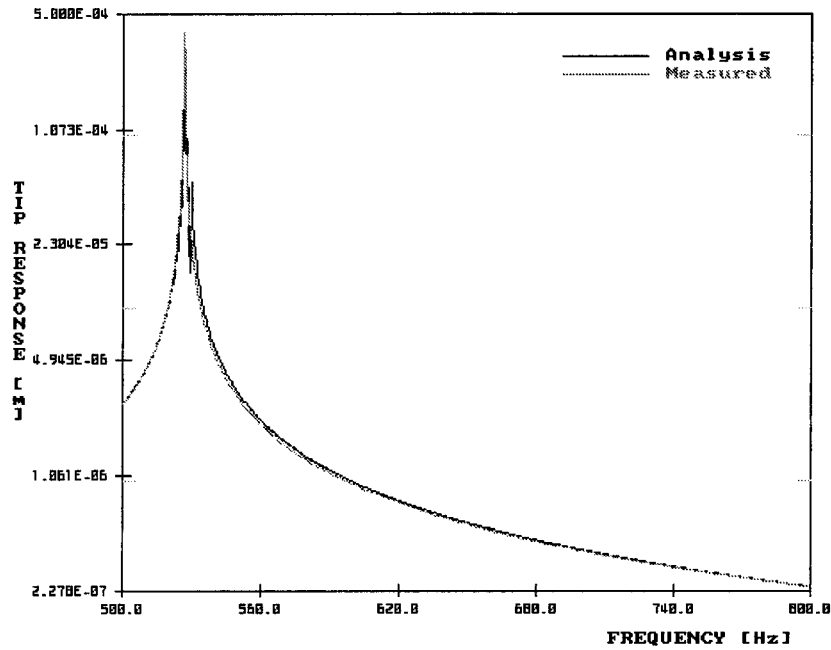
(a)



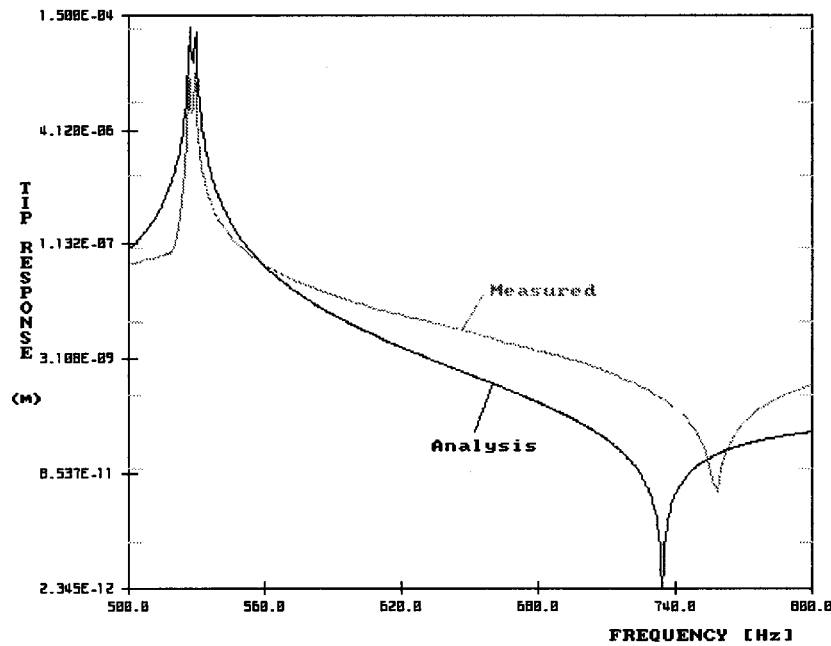
(b)

**Fig. 10 (a) Experimental set-up for simplified blade-damper assembly, (b) finite element model for simplified blade-damper-blade assembly**

(IP mode) is very small, about 4 percent, compared with that for the out-of-phase (OOP) mode. However, the theoretical predictions suggest more than 50 percent natural frequency shift for the same mode when the damper is almost locked at a 100 N normal load. This finding initiated a series of investigations including experimental visualisation of the underplatform dampers under vibration. The results, not presented here, revealed that one of the assumptions made during the theoretical formulation was not valid, i.e., that the damper and the platform surfaces remain parallel and in contact at all times. It has been found that the wedge-shaped dampers cannot always remain parallel to the platform surfaces, as illustrated schematically in Fig. 13(a) where the *rolling* behavior becomes dominant when the relative platform displacement is predominantly radial, as in the case of in-phase (IP) bending modes. The implication of this rolling behavior is that the calculated value for the effective complex stiffness in the local  $y$ -direction ( $k_y^*$ ) is not realistic. This rolling situation has not been



(a)



(b)

**Fig. 11 (a) Comparison of measured and predicted response levels (directly excited blade), (b) comparison of measured and predicted response levels (indirectly excited blade)**

observed, however, when the platforms are subjected to out-of-phase bending vibration hence the theoretical model for complex stiffness in the local  $x$ -direction ( $k_x^*$ ) is valid.

Modeling the rolling behavior depicted in Fig. 13(a) is very difficult and requires much more complicated theoretical models, not only because of the high sensitivity of the rolling effect to the gap between the adjacent platforms but also because of the difficulty in finding the effective contact parameters as a function of the rolling angle, i.e., as a function of contact opening. To date, such a complete theoretical model is not available. In the absence of such a complete theoretical model, the approach adopted here aims to give an allowance for the rolling effect, in the form of a

correction factor as in Eq. (18), based on empirical data combined with a method of estimating a critical platform angle below which the damper motion is predominantly rolling,

$$k_{y,c}^* = f(\beta, \mu) k_y^* \quad (18)$$

where  $k_{y,c}^*$  is the corrected stiffness in the radial direction and  $f(\beta, \mu)$  is the correction factor which is a function of the platform angle and the coefficient of friction and varies between 0 and 1.0. The physical reasoning behind such a correction factor in Eq. (18) is that the damper will slide and follow the imposed platform motion more easily when the roof angle is very small (large plat-

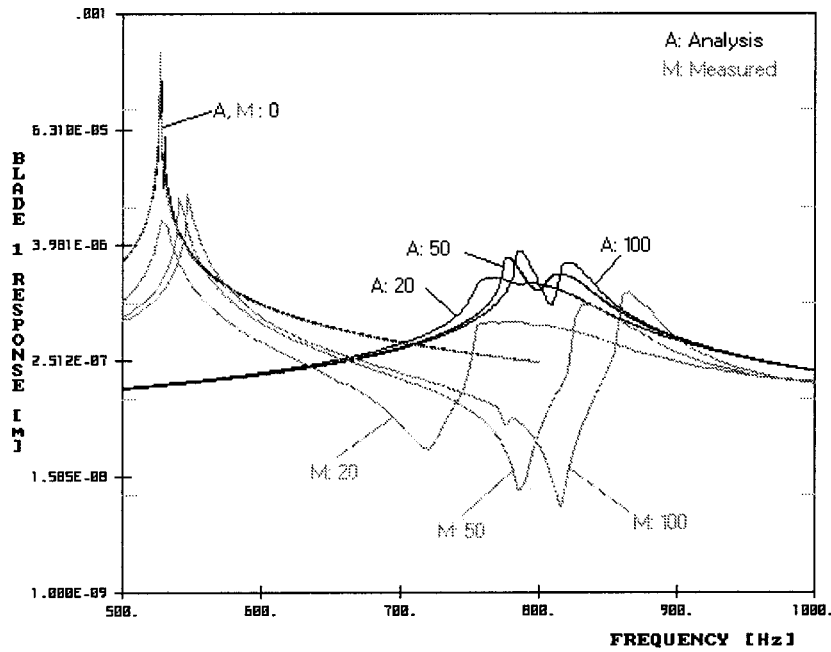


Fig. 12 Initial predictions (damper load=0, 20, 50, 100 N)

form angle). In another words, the damper will predominantly slide rather than roll to follow the platform motion, as in Fig. 13(b), if the platform angle is greater than a critical value.  $\beta_{cr} = \tan^{-1}(\mu)$ . On the other hand, if the platform angle is less than the critical platform angle, for a given coefficient of friction, the damper will tend to roll instead of slide, approaching pure rolling as the platform angle approaches zero degrees (this corresponds to the correction factor being zero). Therefore, there is good justification for the conclusion that the platform angle and the coefficient of friction are critical parameters which should be included in such an approach. The correction factor,  $f(\beta, \mu)$  above, can also be written as a function of normalized platform angle alone, normalization being with respect to critical platform angle. This makes it possible to write the function in terms of  $\beta_N$  only, where  $\beta_N$  is the normalized platform angle. The experimental results of the simplified blade-damper assembly corresponding to the in-

phase bending mode are used to obtain empirical data and the results indicated that the correction factor could be even less than 0.1 for platform angles representative of those dampers currently in use. In the absence of any reliable method, the results obtained using the correction factor are quite useful to identify the extent of rolling for such dampers. Nevertheless, the authors of this paper are aware that a more complicated and complete model needs to be developed in order to avoid the need for the correction factor adopted in this paper. This is one of the areas where the current wedge damper model can be improved significantly.

The theoretical predictions presented in Fig. 12 were recalculated using the correction factor allowing for the rolling behavior and the results are presented in Fig. 14 together with corresponding experimental data. It is immediately seen that the refined analysis can now predict the natural frequency shift for both IP and OOP modes as well as the amount of response reduction and the optimum damping condition. It is also important to note that

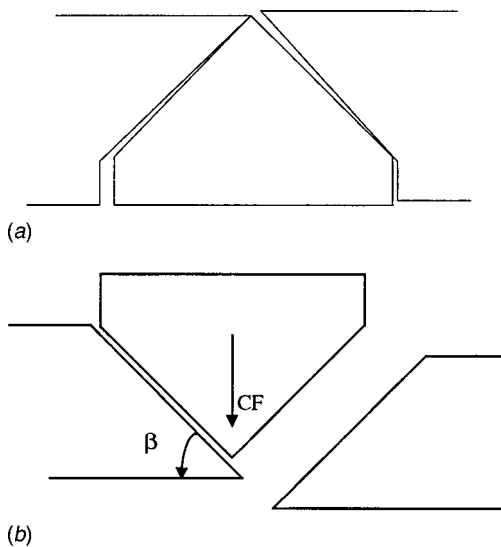


Fig. 13 (a) Relative platform motion in radial direction can cause rolling, (b) damper tends to slide if  $\beta > \tan^{-1}(\mu)$

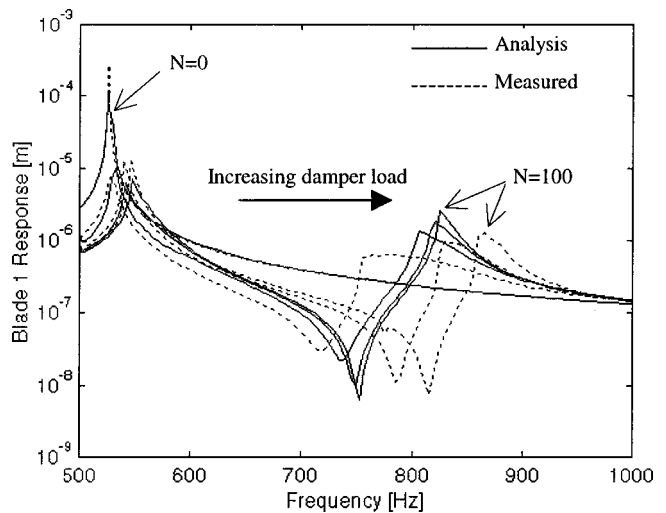
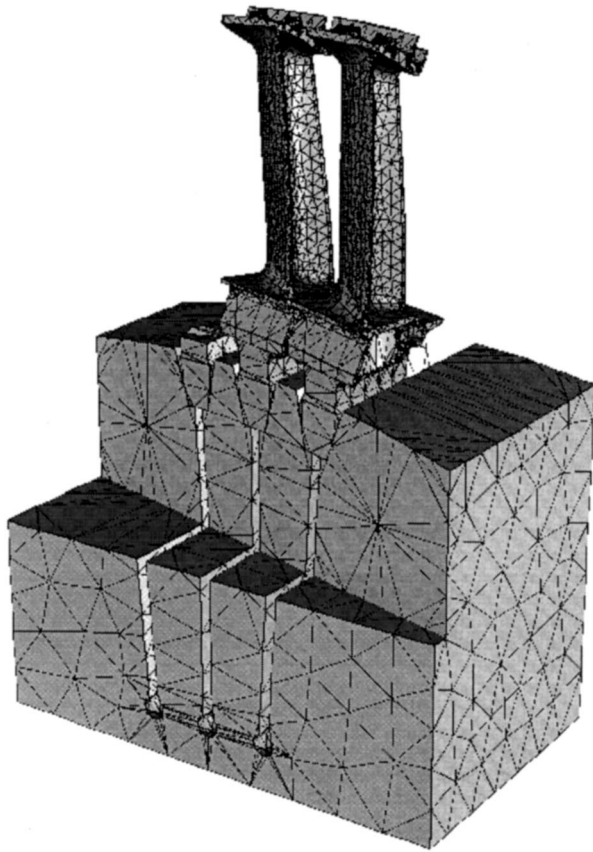


Fig. 14 Comparison of measured and predictions after incorporating rolling effect. (Damper load=0, 20, 50, 100 N.)



**Fig. 15** Finite element model for the linear part of two-blade assembly

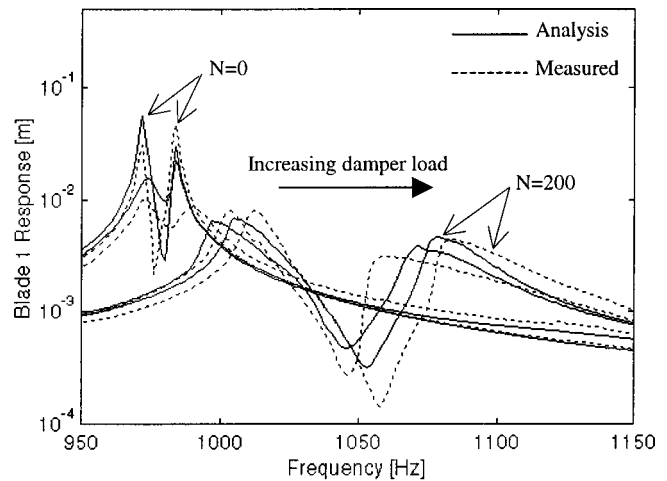
the damper is not as effective in damping the IP mode as it is for the OOP mode. Another point worth stating here is that the curved wedge-shaped dampers do not provide any damping nor natural frequency shift for IP bending mode [18].

**5.2 Case 2: Real Blade-Damper-Blade Assembly.** As illustrated in Fig. 15, this second case study comprised two real turbine blades and a wedge-shaped underplatform damper. The blades were clamped in a slotted block which had root serrations. This holding block was in turn clamped between two large steel blocks, not shown in Fig. 15. Experimental procedure was very similar to the previous case: Damper normal force representing the centrifugal force was achieved via gravitational loading, excitation was applied at about one-third of the blade length from the root, and measurements were taken close the blade tips under constant excitation force of 1N for various values of damper normal force.

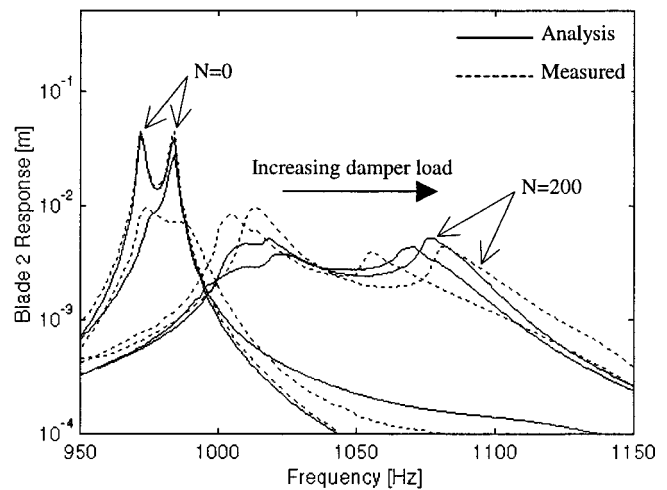
In spite of the geometry being very much complicated than in the previous case, where two simple beams were used, the dynamic behavior of this assembly with real blades and damper was very similar to that of the simple assembly in Section 5.1. As before, the assembly had pairs of in-phase (IP) and out-of-phase (OOP) modes, though the measurements were restricted to a frequency range covering the first IP and OOP bending modes.

Unlike the two-beam assembly, the linear three-dimensional finite element model shown in Fig. 15 for this case was very large, more than 200,000 degrees-of-freedom. However, this was not a drawback as the nonlinear analysis is carried out at active coordinates only as described earlier. Some initial adjustment of the linear model, in terms of material properties and modal damping, was necessary to align the linear model so that linear predictions matched the measurements without the friction damper.

Various input data including measured contact properties,



(a)



(b)

**Fig. 16** (a) Correlation of predictions and experimental data. Directly excited blade,  $F_{ex}=1.0$  N, damper load=0, 10, 100, 200 N. (b) Correlation of predictions and experimental data. Indirectly excited blade,  $F_{ex}=1.0$  N, damper load=0, 10, 100, 200 N.

damper normal load, damper nodes/orientation and platform angle were used to define the damper for nonlinear analysis. The same relationship between the correction factor for rolling and the normalized platform angle obtained from simplified blade-damper assembly study was used here. Response levels were calculated at measurement locations for various values of damper normal loads, keeping the excitation constant as in the experiment. Correlation of the measured and the predicted response levels is presented in Fig. 16 in the form of a series of plots where the damper load is gradually increased. It is seen again that the theoretical predictions correlate very well with the measurements, validating the underplatform damper model and the analysis techniques developed here. An important point to note is that the IP bending mode is affected less by comparison with the OOP bending mode, as found in the previous case. However, the underplatform damper seems to provide a significant amount of damping for the IP mode as well for this assembly, possibly due the IP mode of vibration involving sliding in the local  $z$ -direction.

## 6 Concluding Remarks

1 A theoretical model for wedge-shaped underplatform dampers for turbine blades has been developed. Measured contact parameters can be used to provide the data required to describe contact characteristics.

2 A very efficient frequency domain response analysis method has been proposed. This is based on a combination of harmonic balance method and structural modification approaches. The method allows the calculation of nonlinear response levels at active coordinates only, making it possible to apply the analysis for industrial cases.

3 Wedge-shaped dampers are prone to rolling motion when subjected to radial platform motion and this can reduce the damping in certain modes of vibration usually described as the lower nodal diameter bladed disk modes. Further work is needed to develop a theoretical model for this rolling behavior.

4 The theoretical analysis proposed here can predict the nonlinear response behavior of assemblies with friction dampers with acceptable accuracy. However, an empirical correction factor is needed during this analysis for certain modes of vibration.

## Acknowledgments

The authors are grateful to their sponsors, Rolls-Royce plc, and Volvo Aero Corporation, for their financial support and for permission to publish this work. The authors also thank to J. S. Green of Rolls-Royce, Derby, for generating the finite element mesh for the real blade-damper-blade assembly.

## References

- [1] Griffin, J. H., 1990, "A Review of Friction Damping of Turbine Blade Vibration," *International Journal of Turbo and Jet Engines*, **7**, pp. 297–307.
- [2] Goodman, L. E., and Brown, C. B., 1962, "Energy Dissipation in Contact Friction: Constant Normal and Cyclic Tangential Loading," *ASME J. Appl. Mech.*, **29**, pp. 17–22.
- [3] Iwan, W. D., 1967, "On a Class of Models for the Yielding Behavior of Continuous and Composite System," *ASME J. Appl. Mech.*, **34**, pp. 612–617.
- [4] Rogers, P. F., and Boothroyd, G., 1975, "Damping at Metallic Interfaces Subjected to Oscillating Tangential Loads," *J. Eng. Ind.*, pp. 1087–1093.
- [5] Burtekin, M., Cowley, A., and Back, N., 1978, "An Elastic Mechanism for the Micro-sliding Characteristics Between Contacting Machined Surfaces," *J. Mech. Eng. Sci.*, **20**, No. 3, pp. 121–127.
- [6] Shoukry, S. N., 1985, "A Mathematical Model for the Stiffness of Fixed Joints Between Machine Parts," *Proc. Int. NUMETA Conf.*, J. Middleton and G. N. Pande, eds., Jan., Swansea, UK, A. A. Balkema, Rotterdam, pp. 851–858.
- [7] Sanliturk, K. Y., Stanbridge, A. B., and Ewins, D. J., 1995, "Friction Dampers: Measurement, Modelling and Application to Blade Vibration Control," *Proc. Des. Eng. Conf.*, Vol. 3, Part B, DE-Vol. 84-2, ASME, New York, pp. 1377–1382.
- [8] Menq, C.-H., and Griffin, J. H., 1985, "A Comparison of Transient and Steady State Finite Element Analysis of the Forced Response of a Frictionally Damped Beam," *ASME J. Vib. Acoust.*, **107**, pp. 19–25.
- [9] Chen, S., and Sinha, A., 1990, "Probabilistic Method to Compute the Optimal Slip Load for a Mistuned Bladed Disk Assembly With Friction Dampers," *ASME J. Vib. Acoust.*, **112**, pp. 214–221.
- [10] Wang, J. H., and Chen, W. K., 1992, "Investigation of the Vibration of a Blade with Friction Damper by HBM," presented at the ASME Int. Gas Turbine Aeroeng. Congress & Exhibition, Cologne, Germany, June 1–4, 92-GT-8.
- [11] Cameron, T. M., Griffin, J. F., Kielb, R. E., and Hoosac, T. M., 1990, "An Integrated Friction Damper Design," *ASME J. Vib. Acoust.*, **112**, pp. 175–182.
- [12] Menq, C.-H., Bielak, J., and Griffin, J. H., 1986, "The Influence of Microslip on Vibratory Response, Part I: A New Microslip Model," *J. Sound Vib.*, **107**, No. 2, pp. 279–293.
- [13] Menq, C.-H., Griffin, J. H., and Bielak, J., 1986, "The Influence of Microslip on Vibratory Response, Part II: A Comparison With Experimental Result," *J. Sound Vib.*, **107**, No. 2, pp. 295–307.
- [14] Csaba, G., 1995, "Friction Damping of Turbine Blade Vibrations Using a Microslip Model," *Journal of Machine Vibration*, **4**, pp. 2–7.
- [15] Pfeiffer, F., and Hajek, M., 1992, "Stick-Slip Motion of Turbine Blade Dampers," *Philosophical Transactions of the Royal Society, London*, **A338**, No. 1651, pp. 503–517.
- [16] Sextro, W., Popp, K., and Wolter, T., 1997, "Improved Reliability of Bladed Disks to Friction Dampers," Presented at the ASME Int. Gas Turbine Aeroeng Congress & Exhibition, Orlando, June 2–5, ASME paper no. 97-GT-189.
- [17] Csaba, G., and Andersson, M., 1997, "Optimization of Friction Damper Weight, Simulation and Experiments," presented at the ASME TurboExpo 97, Orlando, FL, June 2–5, 97-GT-115.
- [18] Csaba, G., 1999, "Modelling of a Microslip Friction Damper Subjected to Translation and Rotation," presented at the ASME International Gas Turbine Conference, June Indianapolis, IN.
- [19] Yang, B. D., and Menq, C. H., 1997, "Characterization of Contact Kinematics and Application to the Design of Wedge Dampers in Turbomachinery Blading, Part I and Part II," presented at the ASME TurboExpo 97, Orlando, FL, June 2–5, 97-GT-19 and 97-GT-20.
- [20] Pierre, C., Ferri, A. A., and Dowel, E. H., 1985, "Multi-Harmonic Analysis of Dry Friction Damped Systems Using an Incremental Harmonic Balance Method," *ASME J. Appl. Mech.*, **52**, pp. 958–964.
- [21] Cameron, T. M., and Griffin, J. H., 1989, "An Alternating Frequency/Time Domain Method for Calculating the Steady-State Response of Non-linear Dynamic Systems," *ASME J. Appl. Mech.*, **56**, pp. 149–154.
- [22] Ostachowicz, W., 1989, "The Harmonic balance Method for Determining the Vibration Parameters in Damped Dynamic Systems," *J. Sound Vib.*, **131**, No. 3, pp. 465–473.
- [23] Sanliturk, K. Y., Imregun, M., and Ewins, D. J., 1997, "Harmonic Balance Vibration Analysis of Turbine Blades With Friction Dampers," *ASME J. Vib. Acoust.*, **119**, pp. 96–103.
- [24] Sanliturk, K. Y., and Ewins, D. J., 1996, "Modelling Two-Dimensional Friction Contact and Its Application Using Harmonic Balance Method," *J. Sound Vib.*, **193**, No. 2, pp. 511–523.
- [25] Budak, E., and Ozguven, H. N., 1990, "A Method for Harmonic Response of Structures With Synmetrical Non-linearities," *Proc. 15th International Seminar on Modal Analysis and Structural Dynamics*, P. Sas, ed., Leuven, Belgium, Sept. Katholieke Universiteit Leuven, Leuven, Belgium, pp. 901–915.
- [26] Budak, E., and Ozguven, H. N., 1993, "Iterative Receptance Method for Determining Harmonic Response of Structures With Symmetrical Non-linearities," *Mech. Syst. Signal Process.*, **7**, No. 1, pp. 75–87.
- [27] Tanrikulu, O., Kuran, B., Ozguven, H. N., and Imregun, M., 1993, "Forced Harmonic Response Analysis of Nonlinear Structures Using Describing Functions," *AIAA J.*, **31**, No. 7, pp. 1313–1230.
- [28] Ozguven, H. N., 1987, "A New Method for Harmonic Response of Nonproportionally Damped Structures Using Undamped Modal Data," *J. Sound Vib.*, **117**, No. 2, pp. 313–328.
- [29] Hager, W. G., 1989, "Updating the Inverse of a Matrix," *SIAM Rev.*, **31**, No. 2, pp. 221–239.
- [30] Level, P., Moraux, D., Drazetic, P., and Tison, T., 1996, "On a Direct Inversion of the Impedance Matrix in Response Reanalysis," *Commun. Numer. Methods Eng.*, **12**, pp. 151–159.
- [31] Sanliturk, K. Y., Stanbridge, A. B., and Ewins, D. J., 1996, "Friction Damper Optimization for Turbine Blades: Experiments and Theoretical Predictions," *Proc. 6th Int. Conf. on Vibrations in Rotating Machinery*, Oxford, Sept. 9–12, I. MECH E, London, pp. 171–186, C500/019/96.